SUPPRESSING VORTEX-INDUCED VIBRATIONS VIA PASSIVE MEANS

Hyoungsu Baek & George Em Karniadakis
Division of Applied Mathematics Brown University, Providence, RI 02912, USA

ABSTRACT

We investigate the hydrodynamic effect of a slit in a circular cylinder. The goal of this study is to find a modification of a cylinder to minimize vortex-induced vibrations (VIV). The slit, which is parallel to the incoming flow, is found to be very effective in suppressing vortex shedding and consequently VIV. Through a series of numerical experiments, the optimal size of the slit to suppress the lift force and VIV is obtained. We also find that the slit is more effective at higher Reynolds numbers. A linear stability analysis shows that jet flow though a slit changes the stability behind the cylinder by inducing two small pockets of absolute instability followed by bands of convectively and absolutely unstable regions.

1. INTRODUCTION

Even though numerous techniques to control the drag/lift forces and VIV have been suggested and tested, the study of a cylinder with a slit has not been performed from the VIV suppression point of view. Igarashi (1978) experimentally studied the effect of a slit in a cylinder on the wake flow in the Reynolds number of $O(10^5)$, changing the angle of the slit to the incoming flow from 0 to 90 degrees. He observed slits of angle less than 40 degrees move the vortex formation region downstream and increase the base pressure, while the ones with larger angle decrease the shedding frequency and the base pressure due to the boundary layer suction. Olsen and Rajagopalan (2000) reported an experimental study on the vortex shedding and drag coefficient of circular cylinders with a slit and/or a concave rear notch. They observed higher drag coefficient, and strong and stable vortex-shedding pattern at Re = 2200 for the case of a cylinder with a slit normal to the flow.

In our study, we tested a cylinder with a slit, which was placed at various angles and not necessarily along the diameter, and also a cylinder covered with a thin shell which was dented at various locations with different sizes. Among all designs, a cylinder with a slit parallel to the flow is the most effective in reducing the drag and lift forces and a shrouded cylinder is the second most effective. When vertical or slanted slits are placed along the diameter of, in the frontal section of, or near the base of the cylinder, they show unfavorable effects on the VIV, namely stronger vortex shedding and higher shedding frequency as observed in Igarashi (1978) and Olsen and Rajagopalan (2000). Hence, configurations other than a parallel slit were not further pursued and such results are not presented in the present report.

From the VIV control point of view, a slit in a cylinder can be regarded as a suction-blow method. Since a cylinder with a slit does not require any energy input for operation, the method is similar to Wong's self-sustained fluid injection and Grimminger's guide vane cited in Naudascher and Rockwell (1994). The flow change and control via suction-blow on a bluff body has been reported by many researchers including Dong and Karniadakis (2007); Lin et al (1995); Kim and Choi (2005); and Wood (1964). VIV control via a slit, however, has not been studied. Hence, we carried out numerical simulations at Re = 500 and 1000 with fixed, transverse-free, and free cylinders.

We also employed a local linear stability analysis which was useful in understanding the global behavior of wake. Triantafyllou et al (1986) and Karniadakis and Triantafyllou (1989) showed that the dominant frequency of the wake can be accurately predicted through this stability analysis. For our cases, the linear stability analysis shed some light in explaining the change of the wake flow characteristic.

In this paper, we present a brief account of numerical method and configuration followed by simulation results with fixed, crossflow-free, and totally-free cylinders. Findings from the temporally averaged flow and a local, linear stability analysis are discussed in the section 4. We conclude in section 5.

2. CONFIGURATION AND NUMERICAL METHOD

A slit is placed parallel to the incoming flow along the diameter of a circular cylinder as shown in Figure 1. The width of the slit varies from 0 to 30 % of the diameter of the cylinder. The same configurations were used for stationary and VIV simulations. A typical 2D computational domain for Re = 500 is shown in Figure 1 with $-10 \leq x \leq 50$ and $-10 \leq y \leq 10$. The origin of the coordinate system is located at the center of a cylinder and the positive x axis is pointing downstream.

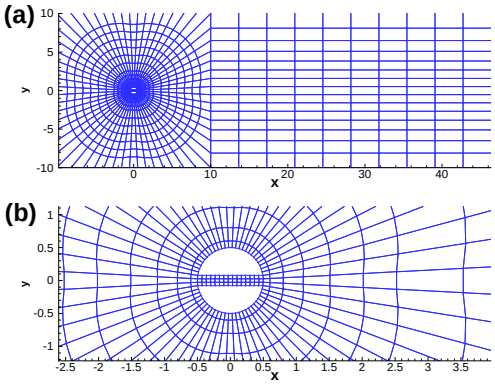

Figure 1: *(a) Domain around a cylinder, (b) Quadrilateral elements in the slit and around a cylinder.*

For stationary cylinders, we solved the Navier-Stokes equations with no-slip boundary condition on a cylinder; the incoming flow is uniformly parallel and steady; the top and bottom sides of the domain have a periodic boundary condition; the outflow is assumed to be fully developed. The incompressible Navier-Stokes equations were solved with NEKTAR, which implements the spectral/hp element method and utilizes the Jacobi polynomial basis to represent the unknowns, velocity and pressure. For more details, we refer to Karniadakis and Sherwin (2005). For the VIV simulation of free cylinders, the Navier-Stokes equations are written in the body-fixed coordinates. The motion of the cylinder is assumed to be linear in both X and Y direction and is described by

$$\ddot{y} + 2\zeta\omega_n\dot{y} + \omega_n^2 y = \frac{f}{m}, \qquad (1)$$

where y denotes either X or Y displacement. The flow/structure systems were weakly coupled by transferring the hydrodynamic forces to the structure solver as external forces after the fluid pressure substep and solving for final viscous substep in the fluid with updated cylinder position and velocity. The XY motions are updated through the 2nd order accurate Newmark integration scheme. For details, we refer to Newman and Karniadakis (1997). The assumption of linear motion of a cylinder and coordinate transformation made the remeshing or interpolation unnecessary even when the cylinder is undergoing large vibrations.

In order to guarantee that our numerical solutions do not depend on the size of numerical domains, we performed *sensitivity tests* with larger numerical domains. The domain is discretized densely inside and near the cylinder boundary so that the elements around a cylinder are fine enough to capture the boundary layer as shown in Fig. 1(b). The numbers of elements range 700 to 1200. At Re = 1000 and VIV simulations, the sizes of domains were increased. In all cases, Reynolds numbers are based on the incoming flow velocity and the cylinder diameter. Most of simulations were done at Re = 500; simulations at Re = 1000 were also carried out in order to verify that slits work at higher Reynolds numbers.

3. VIV CONTROL VIA A SLIT

3.1. Cylinder - Fixed

We fist investigate the effect of a slit in a stationary cylinder on the lift force in uniform flow at Re = 500 and 1000. Table 1 shows simulation cases with varying slit ratio, s/D, where s and D are the slit width and the diameter of a cylinder, respectively. Case ST1, $s/D = 0.0$, is the uncontrolled reference case. Quantitatively speaking, the flow through the slit moves the vortex formation downstream and disturbs the symmetry of the vortex shedding through interactions of shear vortices from the slit with those from the wall. When vortices from the slit are not

Cases	s/D	f_1	f_2	f_3	f_4
ST1	0.0	0.235	$3f_1$		
ST2	0.05	0.233	$3f_1$		
ST3	0.12	0.210	$3f_1$		
ST4	0.14	0.249	$3f_1$		
ST5	0.16	0.265	$f_1/4$	0.579	0.767
ST6	0.20	0.092	$3f_1$	0.465	0.625
ST7	0.30	0.142	$f_1/2$	0.027	$2f_1$

Table 1: *Peaks at the power spectrum of the lift force in a stationary cylinder at Re = 500.*

strong ($s/D < 0.16$), they only contribute to the stretching of shed vortices from the cylinder and disappear in the near-wake. In case ST5, the vortices from both sides of cylinder are stretched farthest; the vortex formation location is also pushed downstream; the lift force becomes minimal. When $s/D > 0.16$, vortices from the slit are shed and merged to the vortices of the same or opposite sign from the cylinder wall. Hence, the vortex street becomes very irregular and the periodicity of the lift and drag forces disappears. Cases ST6 and ST7 demonstrate that the symmetric break down of the jet through the slit induces symmetric vortex shedding before the flow reaches the steady state. Even in steady state, there are time intervals during which the vortex shedding becomes symmetric. The drag and lift

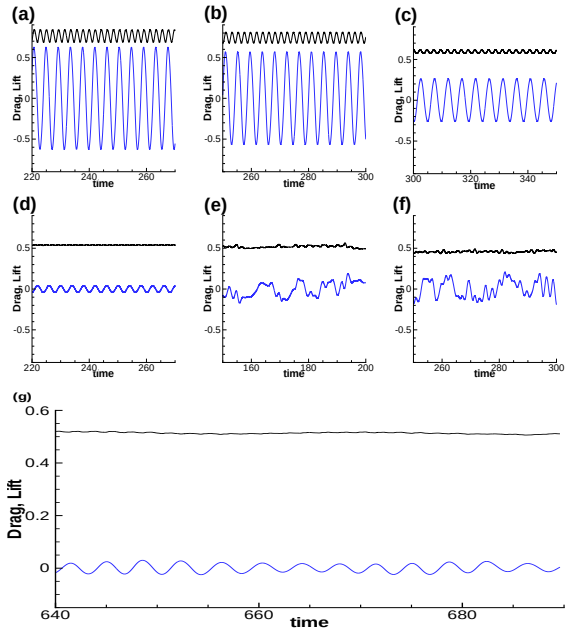

Figure 2: *Drag and lift forces versus time: (a) ST1, (b) ST2, (c) ST3, (d) ST4, (e) ST6, (f) ST7, (g) ST5 at* $Re = 500$.

force time histories in Figure 2 show the dramatic changes of the lift forces as the slit ratio increases. The periodicity of the vortex shedding of case ST5 still seems to have the dominant single frequency component in the lift. The lift force amplitude, however, reduces to less than 10 percent of that of the reference cylinder. For those with larger slit ratio than 0.16, the drag and force time histories become chaotic due to competition between antisymmetric Karman vortex shedding mode from the cylinder and the symmetric shedding mode from the jet.

We calculated the RMS values of the lift force time history to compare the energy among the cases. We want to point out that the RMS of case ST7 is larger than that of case ST6. The

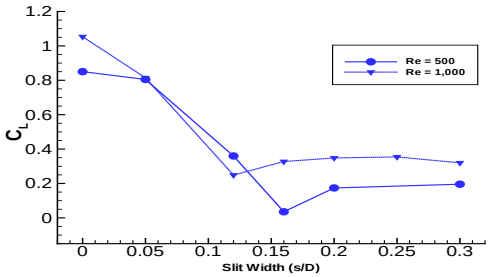

Figure 3: *RMS lift coefficients versus the slit width at* $Re = 500$ *and 1000.*

RMS lift coefficient diminishes up to the slit ratio 0.16 and then increases slightly as the slit ratio increases further. The increase of RMS lift coefficient agrees with the amplitude increase in the lift force time history. We confirmed that this optimum slit size becomes smaller when the Reynolds number increases as shown in Figure 3. The frequency spectrum of the lift force time

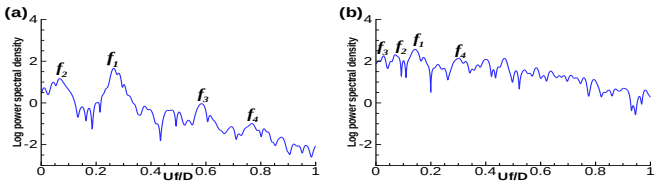

Figure 4: *Lift force power spectrum: (a) ST5, (b) ST7 at* $Re = 500$.

history reveals that the superharmonics of the vortex shedding frequency disappear gradually as the slit ratio increases. It is noteworthy that up to $s/D = 0.12$, the dominant shedding frequency listed in Table 1 gets smaller from $f = 0.235$ to $f = 0.210$. Case ST4 shows that frequency components between two peaks start to grow. The force spectrum of case ST5 shown in Figure 4 loses most of strong peaks associated with the reference cylinder. Cases ST6 and ST7 lose those peaks completely. The spectral analysis agrees with the time history of the lift force and confirms the *detuning process* of the slit more clearly. However, drastically reduced lift forces with persistent dominant frequency in cases ST4 and ST5

seem to explain that the suppression of the lift force is induced mainly from the longer vortex formation length and that the detuning is an outcome of such change in the wake.

3.2. Cylinders - Y only VIV

We also performed simulations of a rigid 2D cylinder, which is allowed to move along the Y direction. For VIV simulations, three parameters are necessary to define the property of a cylinder: mass ratio, damping, and natural frequency. The natural frequency of a cylinder, $\omega_n = 2\pi \cdot 0.225$, is chosen to be close to the non-dimensional vortex shedding frequency of a fixed cylinder at Re = 500. Since the positive damping decreases the VIV of a cylinder, the damping coefficient was set to 0 or 0.01 to maximize the motion. The mass ratio is set to 3, which is close to the density ratio of pipes used in the ocean. With these fixed parameters, simulation cases with different slit ratios are listed in Table 2.

Cases	s/D	f_1	f_2	f_3	f_4
VY1	0.0	0.230	$2f_1$	$3f_1$	$4f_1$
VY2	0.12	0.218	$3f_1$	0.783	0.956
VY3	0.16	0.275	0.221	0.079	0.624
VY4	0.20	0.077	0.202	$7f_1$	
VY5	0.30	0.177	$f_1/3$	0.294	

Table 2: *Peaks at the power spectrum of Y displacement of Y only VIV. In all cases, Re = 500, damping 0.0, and mass ratio 3.*

More simulations with larger mass were done but we present only the cases of mass ratio 3 since cylinders with the larger mass ratio show smaller amplitudes. In the cases VY1 and VY2, positive structural damping coefficient caused reduction of the amplitude of the motion by 10 %. The Y motion almost disappears in case VY3 as shown in Figure 5.

The power spectrum of the cylinder motion in Y direction as shown in Figure 6 demonstrate a similar trend to the one observed in the fixed cylinder cases. The strong energy around the superharmonics of shedding frequency spreads out to surrounding frequencies gradually as the slit ratio increases.

3.3. Cylinder - XY VIV

Encouraged by the results of the Y direction VIV simulations, we also performed VIV simulations with free cylinders listed in Table 3.

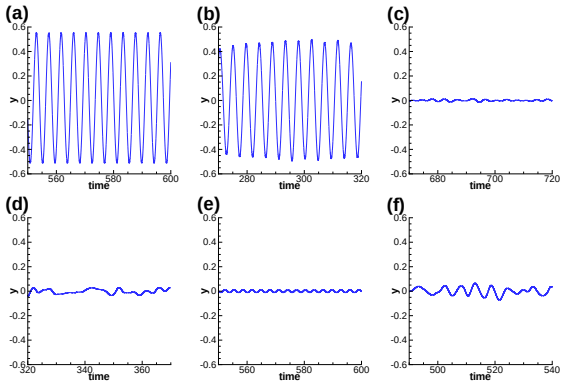

Figure 5: *Cylinder Y displacement versus time: (a) VY1, (b) VY2, (c) VY3, (d) VY4, (e) VY4 with damping = 0.01, (f) VY5.*

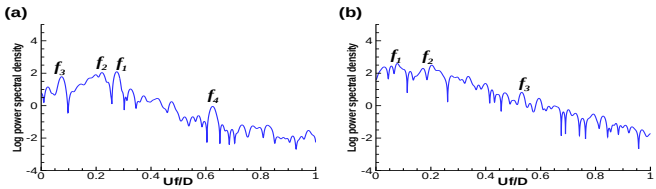

Figure 6: *Spectrum of Y displacement of (a) VY3 and (b) VY4.*

In cases VXY1 and VXY2, positive structural

Cases	s/D	f_1	f_2	f_3	f_4
VXY1	0.0	0.230	$2f_1$	$3f_1$	$4f_1$
VXY2	0.12	0.216	$f_1/3$	0.363	$3f_1$
VXY3	0.16	0.216	0.279	0.589	0.792
VXY4	0.20	0.062	0.196	0.327	
VXY5	0.30	0.174	0.323	0.488	

Table 3: *Peaks at the spectrum of Y motion in XY VIV simulations. In all cases, Re = 500, damping 0.0, and mass ratio 3.*

damping reduces the motion amplitudes of undamped cylinders by 10 %. Figure 7 shows that case VXY3 with $s/D = 0.16$ is still effective in suppressing the XY motion as well as Y motion. Due to eventual detuning, the limit cycle of the cylinder is a fixed point. As observed in the cases of Y VIV simulations, the spectral analysis of the Y displacement reveals that the detuning is taking place from case VXY2 and the vortex shedding superharmonics disappear in case VXY5 completely as shown in Figure 8. Both

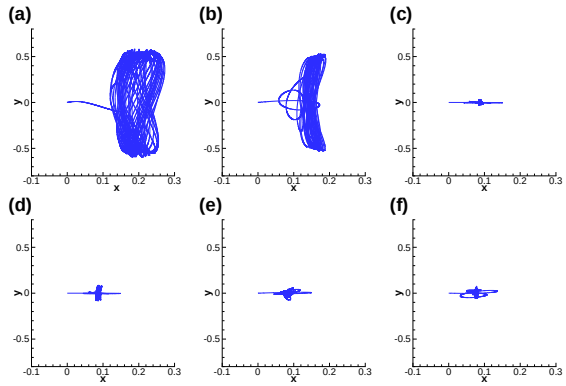

Figure 7: *Cylinder displacement trajectories in X-Y plane: (a) VXY1, (b) VXY2, (c) VXY3, (d) VXY3 with damping = 0.01, (e) VXY4, (f) VXY5.*

Y only and XY VIV simulations start from the fully developed flow with the cylinders fixed at the origin. Subsequently, cylinders were released to allow motion along either Y only or XY direction.

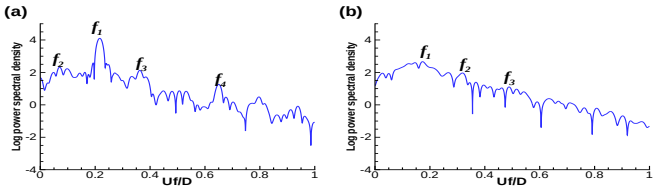

Figure 8: *Spectrum of Y motions of case (a) VXY2 and (b)VXY5.*

4. LINEAR STABILITY ANALYSIS

We carried out a stability analysis of the wake flow using local, linear stability theory. During fixed cylinders simulations, temporal averages of flow fields were obtained and the u velocity profiles at different x stations in the wake were extracted. These velocity profiles were used as a base profile for the stability analysis under the assumption that crossflow is negligible and the streamwise change of the velocity profile is not significant. The inviscid Orr-Sommerfeld equation is solved numerically to find the dispersion relation as in Triantafyllou et al (1986), $\omega = \omega(k)$, which maps k_i constant lines onto the ω plane at $x/D = 0.7, 0.8, ..., 2.6$. From the similarity in the shape of the quadratic mapping, we identify double root; the sign of the imaginary part determines whether the flow is convectively or absolutely unstable. If the double root (which looks like a cusp on the ω plane) is above the ω_r axis, the instability is absolute. If it is below the ω_r axis, it is convective.

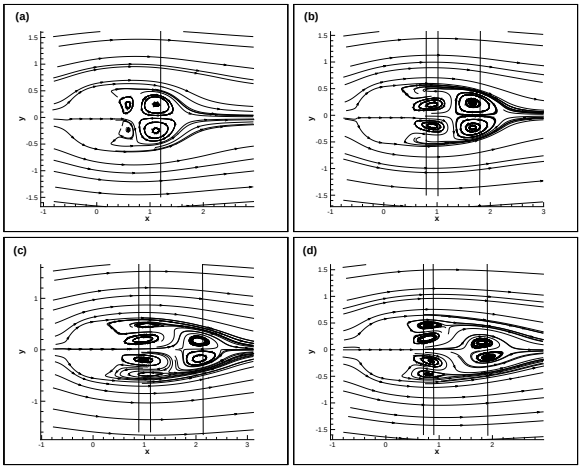

Figure 9: *Stream lines drawn from average velocity field: (a) ST3, (b) ST4, (c) ST5, (d) ST6. The vertical lines indicate the location where the linear stability analysis predicts the strongest local absolute instability.*

Streamlines in the averaged flow fields show very interesting change of the fields as the slit width increases. It is obvious from Figure 9 that the recirculating zones near the base of the cylinder get stretched and intensified. The vortex systems are shifted downward farthest for case ST5. Vertical lines shown in Figure 9 indicate the locations of local maxima of disturbance growth rate predicted with the stability analysis. Their locations coincide with the centers of the vortex systems with a small offset.

The stability analysis with the reference cylinder was performed as a benchmark test and it predicts the Strouhal number, 0.2476, which differs from the vortex shedding frequency, 0.2345, by 5.2 %. The growth rates of absolute instability are shown in Figure 10. As the slit width increases, however, the temporal wave numbers at the double roots could not be directly related to the Strouhal number. For cases ST4, ST5, and ST6, the map of constant k_i lines have two pinch points (double root of $\omega(k) = 0$) and this seems to be related to the vortex system induced by the jet flow through the slit. Case ST3 shows that the absolute instability zone is shifted downward even though the max growth rate is larger

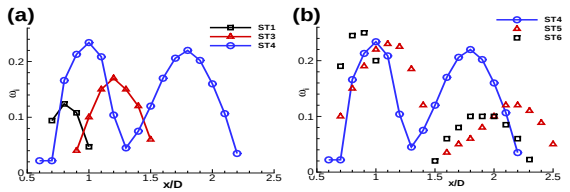

Figure 10: *Peak growth rate(ω_i) versus x/D: (a) ST1, ST3, ST4, (b) ST4, ST5, ST6*

than that of case ST1. In cases ST5 and ST6, two absolute instability pockets shown as humps in Figure 10 are getting closer to the cylinder while they are separated by a band of convective instability. As s/D increases, this band gets wider along the streamwise direction. Qualitatively, those observations agree with the vorticity distribution

5. CONCLUSIONS

We investigated the hydrodynamic effect of slits in a 2D circular cylinder on the wake flow and VIV. A slit is placed parallel to the incoming flow along the diameter of the cylinder, and with width varied from 0 to 30 % of the diameter of the cylinder. The effect of slit was tested for both fixed and free cylinders with high-order spectral/hp element method. Systematic numerical simulations demonstrated that a slit parallel to the incoming flow is a very efficient way in suppressing the lift and VIV by modifying the wake flow. The existence of optimal slit width at Re = 500 and 1000 shows that the reduced drag and lift are ascribed not to the reduced frontal area but to the change of instability regions and their interactions. Modified cylinders with a slit of sufficiently large width make a strong jet flow into the wake and changes the vortex shedding pattern dramatically. For the slit width of larger than 16 % of the diameter, instantaneous flow field does not show periodic vortex shedding pattern any more.

In the time-averaged flow, slits make two additional vortex systems behind the pieces of a cylinder while shifting downstream and shrinking the original ones observed in the near-wake of an unmodified circular cylinder. A local linear stability analysis was carried out to find the changes in the size and location of the absolute instability zones even though the resulted multiple frequencies could not be predicted directly from the analysis.

6. ACKNOWLEDGEMENTS

This research was supported by ONR and VIV simulations were performed on the IA-64 TeraGrid Linux Cluster systems at NCSA and SDSC.

7. REFERENCES

Dong, S., Karniadakis, G. E., 2007, Suppressing the fluctuating lift on a circular cylinder. *Phys. Rev. Lett.* under review.

Igarashi, T., 1978, Flow characteristics and a circular cylinder with a slit. 1st report, flow control and flow patterns. *Bulletin of JSME* **21**: 656-664.

Karniadakis, G. E., Sherwin, S. J., 2005, Spectral/hp element methods for CFD. *Oxford University Press*

Karniadakis, G. E., Triantafyllou, G. S., 1989, Frequency selection and asymptotic states in laminar wakes. *J. Fluid Mech.* **199**: 441-4469.

Kim, J., Choi, H., 2005, Distributed forcing of flow over a circular cylinder. *Physics of Fluids* **17**: 033103-1 - 033103-16.

Lin, J. C., Towfighi J., Rockwell D., 1995, Near-wake of a circular cylinder: control by steady and unsteady surface injection. *Journal of Fluids and Structures* **9**: 659-669.

Naudascher E, Rockwell D., 1994, Flow-induced vibrations: an engineering guide. *A.A. Balkema*

Newman, D., Karniadakis, G. E., 1997, A direct numerical simulation study of flow past a freely vibrating cable. *J. Fluid Mech.* **344**: 95 - 136.

Olsen, J. F., Rajagopalan S., 2000, Near-wake of a circular cylinder: control by steady and unsteady surface injection. *Journal of Wind Engineering and Industrial Aerodynamics* **86**: 55-63.

Triantafyllou, G. S., Triantafyllou, M. S., Chryssostomidis, C., 1986, On the formation of vortex streets behind stationary cylinders. *J. Fluid Mech.* **170**: 461-477.

Wood, C. J., 1964, The effect of base bleed on a periodic wake. *Journal of the Royal Aeronautical Society* **68**: 447-482.